Indonesian Geotechnical Journal, April 2025, Vol 1 (1). Page 1-14
DOI: https://doi.org/10.56144/igj.v4i1.115
E-ISSN:2829-7520
https://indonesian-geotechnical-journal.org/index.php/JGI/issue/archive

Application of Terrestrial Laser Scanning and 3D Finite Element Analysis to Safety Assessment of a Roller-Compacted Concrete Dam

Nguyen Hoang Pham[1], Tuan-Nghia Do[2,*], and Lan Chau Nguyen[3]
[1]Faculty of Civil Engineering, Thuyloi University, 175 Tay Son, Hanoi, Vietnam; hoang.kcct@tlu.edu.vn
[2]Faculty of Civil Engineering, Thuyloi University, 175 Tay Son, Hanoi, Vietnam; dotuannghia@tlu.edu.vn
[3]Faculty of Civil Engineering, University of Transport and Communications, 3 Cau Giay, Hanoi, Vietnam; nguyenchaulan@utc.edu.vn
*Correspondence: dotuannghia@tlu.edu.vn

SUBMITTED 20 March 2025 **REVISED** 7 April 2025 **ACCEPTED** 29 April 2025

ABSTRACT This paper presents the combination of terrestrial laser scanning (TLS) and 3D finite element analysis to assess safety of a roller-compacted concrete (RCC) dam. The investigated case is the Ban Lai dam, located in Lang Son province, Vietnam. The deformations of the dam surface at three different storage water levels were firstly scanned by point cloud through TLS and then back analyzed using the 3D finite element software (Plaxis). The numerical analysis was adopted to calculate vertical normal stress and horizontal normal stress along the stream direction caused by the dam deformation in order to assess its safety during operation. Results showed that the dam surface's deformations by the numerical analysis and TLS were very close to each other and also approximate to those of total station. When the storage water level rose, both the maximum (tensile) normal stresses and the minimum (compressive) normal stresses decreased but the dam remained at a safe state. The constructed relationship between the vertical and horizontal normal stresses with the storage water level could help to roughly determine the normal stress corresponding to any storage water level and judge the safety of the dam. Finally, a flow chart of the integration between TLS and 3D finite element analysis was proposed to assess dam safety for other cases.

KEYWORDS roller-compacted concrete (RCC) dam; 3D finite element analysis; deformation monitoring; terrestrial laser scanning (TLS); safety assessment

1 INTRODUCTION

So far, the terrestrial laser scanning (TLS) technique has been used widely in 3D surveying of various structures, including building, dam, bridge, etc., due to its simplicity. This technique has been studied by many researchers such as Shen et al. (2023), Oytun and Atasoy (2022), Jiang et al. (2021), Aryan et al. (2021), Muralikrishnan (2021), Kaczmarek et al. (2019), Antova (2015), etc. In principle, a scanner generates a pulsed laser towards the target object and then retrieves the returned pulse of the laser. The distance from the scanner to the target object surface can be calculated automatically through the round-trip time of one pulse of the laser. By generating many pulsed lasers towards the target object, the scanner is able to record the point cloud of the target object surface if its location is validated. Due to the fast-traveling velocity of the laser, the scanner can finish scanning any surfaces within very short time. The TLS technique has many advantages as compared with traditional measurement method including: (1) Quick surveying time; (2) High accuracy; and (3) Output data is stored in point cloud. Many researchers have adopted this technique to predict the dam deformation during operation based on statistical regression analyses, such as Xiao et al. (2022), Hu and Wu (2019), Gu et al. (2020), Zhao and Wu (2021), etc., or through machine learning methods, such as Su et al. (2016; 2018a; 2018b), , Dai et al. (2018), Gu et al. (2021; 2022), He et al. (2018), Zhao and Wu (2021), etc.

On the other hand, in order to assess the dam safety, it is necessary to perform numerical analysis to clarify the stress state inside the dam body and its foundation. The numerical model was first calibrated by the measured deformation from stations inside the dam and then the stress state of the dam was calculated at different water levels to compare the maximum compressive and tensile stresses with the allowable ones of the dam material. This routine of investigation was performed by many researchers, such as Zhan et al. (2023), Hemeda, S. (2022), He et al. (2022), etc. Due to the fact that most of the previous research employed the measurement data provided by the monitoring stations inside the dam, such as inclinometer, although the data is of high quality, care should be taken to maintain or replace the monitoring stations. Moreover, measurement inside the dam could not cover the whole dam area unlike the TLS technique. Therefore, by integrating the data provided by TLS technique and 3D numerical analysis, a more comprehensive safety evaluation of a dam can be achieved.

In this study, the deformation of Ban Lai dam, a roller-compacted concrete (RCC) dam, in Lang Son, Vietnam at different storage water levels was measured using the 3D TLS technique. Then, 3D stress deformation analysis would be performed to determine the stress state of the dam based on the TLS measurements for safety evaluation. Finally, a flow chart to integrate the TLS measurements and 3D numerical analysis was proposed to assess dam safety for other cases.

2 STUDY AREA

The Ban Lai dam was constructed in 2021 and is located on the Ky Cung river in Lang Son province, Vietnam. Figure 1 shows the perspective and front views of the dam after construction. The Ban Lai reservoir is responsible for food control, irrigation, power generation, and water supply within Lang Son province. The total storage capacity is 1.55×10^8 m^3. The reservoir's dead storage level, normal storage level, design flood level, and check flood level are +294.50 m, +303.10 m, +314.21 m, and +314.25 m, respectively. As shown in figure 2, the Ban Lai dam is 55.7 m high (can add the top elevation of the dam here) and 372 m long, which is made from RCC M15. The dam's width is 10 m at the top and 34.8 m at the bottom with the triangle extension at the downstream side. The spillway section (located in the middle of the dam) consists of 3 deep discharge openings and 2 surface discharge gates. Each of the openings is 5 x 3.5 m with a spillway crest at +294 m. The gates are located above the openings with 12 m width each and a spillway crest at +303.10 m. The dam has a water intake culvert with a flow rate of 25.32 m^3/s. There is a hydropower plant with a capacity of 7,000 kW using the discharge stream. The reservoir is capable of receiving water from a catchment area of 457 km^2.

Figure 1. The Ban Lai dam after construcion: (a) Perspective view and (b) Front view

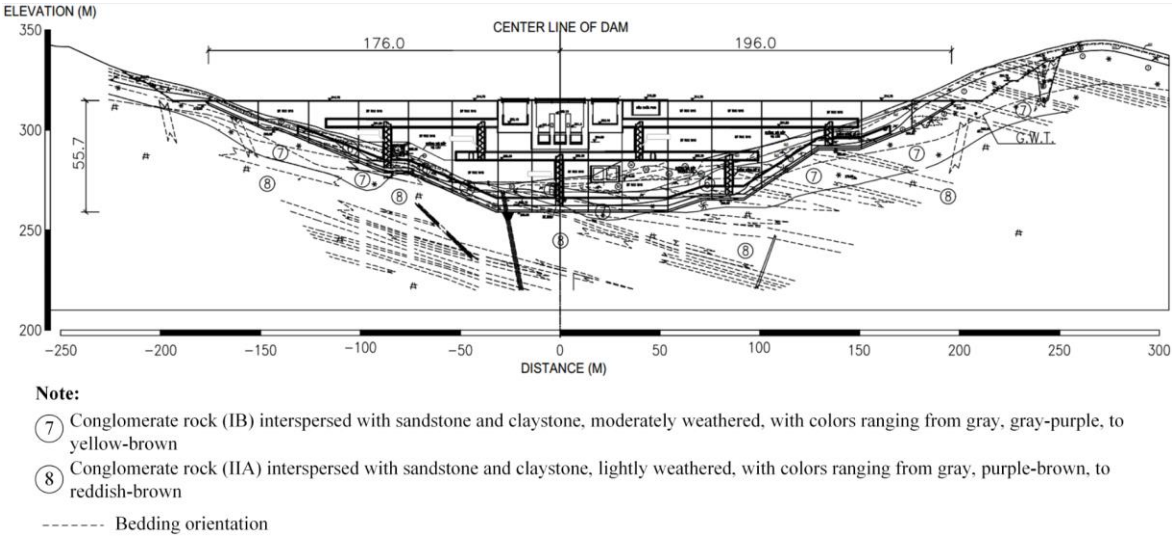

Figure 2. Profiles of the Ban Lai dam and soil stratigraphy

Figrue 2 also presents profile of soil stratigraphy beneath the dam. The dam was placed within rock layer 7 and 8. Rock layer 7 (IB) is conglomerate rock with thickness ranging from 3 m to 26 m, which is interspersed with sandstone and claystone, moderately weathered, with colors ranging from gray, gray-purple, to yellow-brown. The rock has undergone significant color changes, is heavily cracked, and the fracture surfaces are often open and coated with iron oxide. The rock is relatively hard, with broken pieces that are poorly defined, and the rock's strength is uneven. Rock layer 8 (IIA) is located beneath rock layer 7, which is more than 50 m thick. This layer is also conglomerate rock, which is interspersed with sandstone and claystone, lightly weathered, with colors ranging from gray, purple-brown, to reddish-brown. However, the rock is generally unaffected by significant alteration, with minor weathering present. It is characterized by hardness, angular fragmentation, and moderate fissuring. Properties of the rock layers 7 and 8 are summarized in Table 1. Note that the cohesion and internal frictional angle were estimated based on the weathering level of rock according to the Vietnamese code TCVN 4253-2022. The compressive strength was determined from unconfined compression test.

Table 1. Properties of rock layers

Parameter	Symbol	Unit	Rock layer 7	Rock layer 8
Dry unit weight	γ_d	kN/m^3	25.3	25.5
Specific gravity	G_s		2.76	2.76
Poisson's ratio	ν		0.37	0.33
Cohesion (rock block)	c'	kPa	150	300
Internal frictional angle (rock block)	ϕ'	^{0}	32	40
Cohesion (rock-concrete)	c'	kPa	180	320
Internal frictional angle (rock-concrete)	ϕ'	^{0}	30	37
Compressive strength	R_n	kN/m^2	58250	73220
Young's modulus	E	kN/m^2	4x10^6	7x10^6

3 METHODOLOGY

3.1 Terestrial Laser Scanning

Terrestrial laser scanning (TLS) is a relatively recent surveying technique in geodesy. In principle, the scanner emits a pulsed laser that illuminates the target object and measures the neccessary time for the laser to return. By calculating the round-trip time of the pulsed laser, the TLS can automatically calculate the distance between itself and the target object surface, which is also known

as a time-of-flight (TOF). Since TLS can capture dense point clouds in a very short time, modern laser scanners offer significantly faster data acquisition speeds as compared with traditional surveying tools like total stations (Xu et al. (2019); Abellan et al. (2011). Besides, The RGB color data of the target object is also can recorded by TLS. Provided that the center of the laser scanner is the origin of the Cartesian coordinate system, the coordinates of points on the target object surface in the 3D space can be constructed through the distance between them and the scanner in associated with the inclined angle of the laser pulse (Yue et al., 2010). The GLS-2200 pulse-based scanner, manufactured by Topcon, was adopted to scan the Ban Lai dam surface in this study. The main technical characteristics of this scanner are summarized in Table 2. The scanner can measure from a distance of 40 m to 500 m, with maximum scanning rate of 120000 points per second, corresponding to laser class 3R. The minimum spot size is 4 mm and the minimum point increment is 3.1 mm. The scanner has a field of view of 270^0 in vertical direction and 360^0 in horizontal direction (i.e., full rotation). The maximum distance accuracy is 3.1 mm. The above technical characteristics enable a high accuracy of the scanning survey in this study.

Table 2. Main technical characteristics of GLS-2200 laser scanner

STT	Type	Characteristics
1	Maximum range (90% reflectivity)	500 m
2	Maximum measurement rate	120000 points/sec
3	Laser class	Class 3R
4	Minimum spot size	4 mm
5	Minimum point increment	3.1 mm at 10 m
6	Maximum point number	V:15202 Points/Line (270°) H:20268 Points/Line (360°)
7	Field-of-view	V:270°/ H:360°
8	Angle accuracy	H: 6” / V: 6”
9	Distance Accuracy	3.1 mm
10	Surface Accuracy	1.0 mm
11	HDR camera	Wide : Diagonal 170° Tele. : 8.9°(V) x 11.9°(H) Both Wide & Tele.: 5 Megapixels
12	Tilt Sensor	Liquid 2-axis tilt-sensor Compensation Range: ± 6’
13	Operation temperature	-5 ^{0}C to +45 ^{o}C

TLS was conducted during the operation of the dam. Since the dam is 55.7 m high and 372 m long, acquiring a comprehensive point cloud of the entire surface with a single scan is not feasible. Therefore, multiple scans were executed to improve the accuracy of TLS through overlapping different data sets.

Figure 3 shows the six scans that were conducted at six distinct stations surrounding the dam for the first time corresponding to storage level of +295.1 m. For each scan, the scanner was positioned at the observation station, and its coordinates were determined based on the established geodetic network, which helped to obtain more accurate coordinates of the scanner and reduce alignment error. The scanner normally performed 360^0 scanning within five minutes. In the first scan, the scanner recorded one hundred and fifty million points in total, which served as the reference point cloud. The point cloud plot is shown in figure 4. The second and third measurement campaigns were conducted when the storage levels were +300.9 m and 307.95 m using the same methodology as the first one.

Figure 3. 3D model of the Ban Lai dam (rendered view)

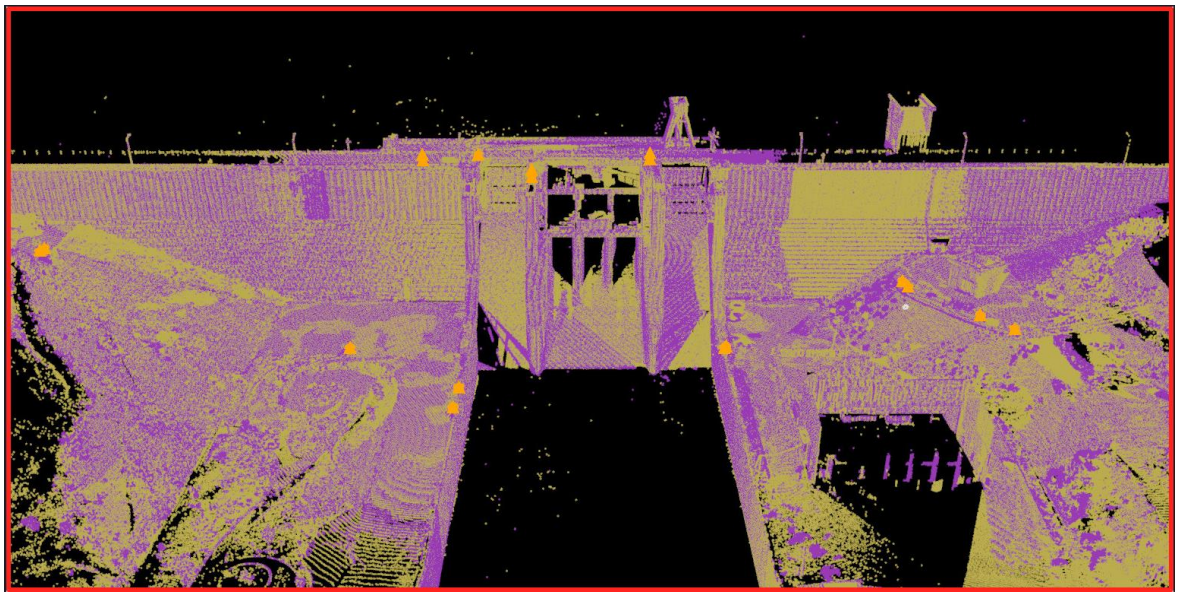

Figure 4. Point cloud of the Ban Lai dam at storage level of +295.1 m.

The MAGNET Collage software was employed to preprocess these three sets of TLS data. It was required to first extract the geodetic coordinates of each scanner based on the established geodetic network and then assign the geodetic coordinates of the scanner center by adding the scanner's height. Hence, the software can determine the location of each scan center through the backsighting orientation function. At each scanning, the alignment of the partial scans was performed, creating a single point cloud data set consisting of all scanned points with overall standard deviation of 0.0008 m. Three point cloud data sets were constructed corresponding to the three measurement times. Figure 5 is the differential deformation shading plot of the Ban Lai dam along the stream direction at the storage levels of +300.9 m and 307.95 m as compared with that at +295.1 m.

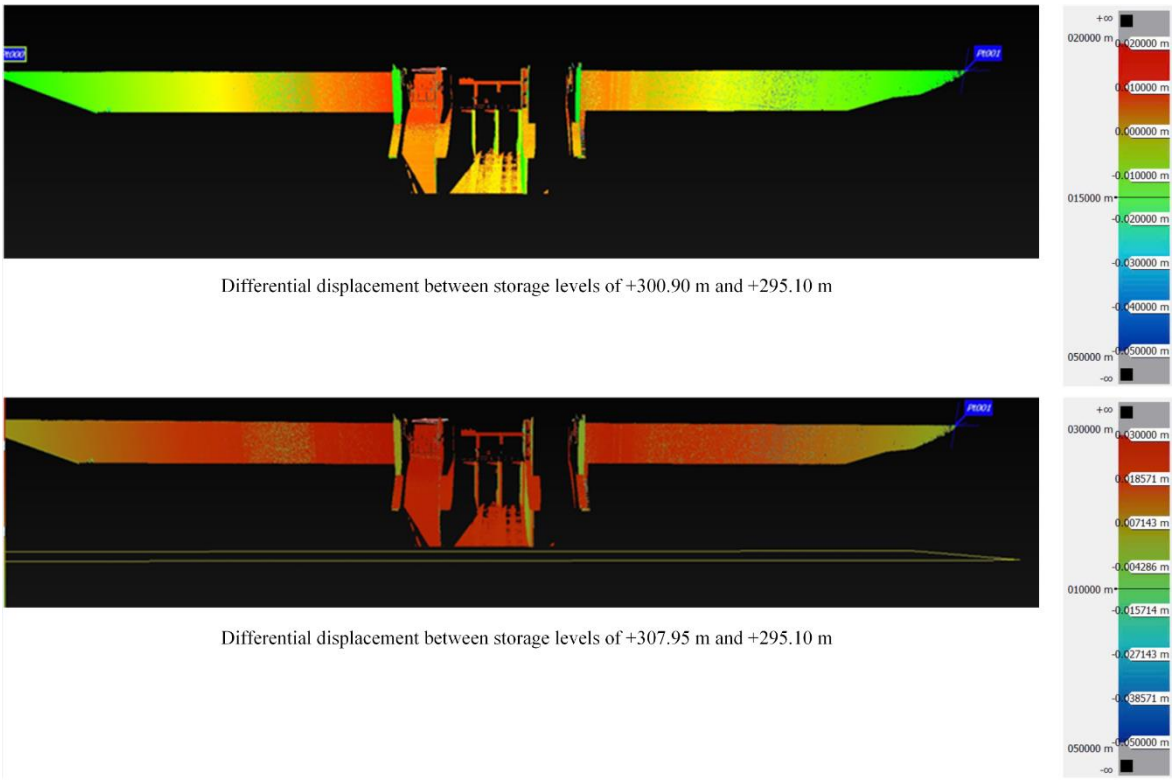

Figure 5. The differential deformation shading plot of the Ban Lai dam along the stream direction at the storage levels of +300.9 m and 307.95 m as compared with that at +295.1 m.

3.2 Back Analysis

Plaxis software was adopted to perform 3D back analysis in this study. This software is built on the basis of the finite element method, which is capable of modelling the complicated stratigraphy, advanced behaviors of soil/rock, and interaction between structure and surrounding soil/rock for various structures (Ezzeldin et al. (2024); Ledesma et al. (2022); Liu et al. (2022); Maddah et al. (2021)). Figure 6 is the 3D finite element model of the Ban Lai dam. As shown in this figure, the model dimension is 500x130x100 m with 151930 elements, simulating the whole dam. The adopted element is a quadratic 15-node triangular one with 3 corner nodes and 12 additional mid-side nodes, placed on the edges of the element. It enables the quadratic interpolation between points within the element, leading to smoother and more precise results, especially for problems with complex geometries or varying material properties.

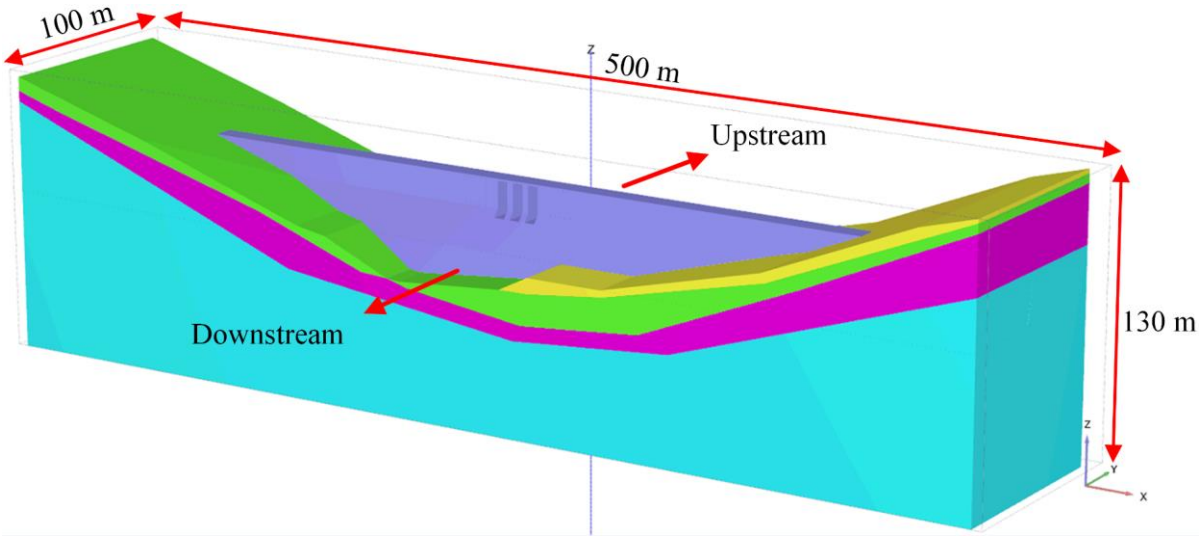

Figure 6. 3D finite element model of the Ban Lai dam

It was assumed that the behaviors of the dam material and the rock layers 7 and 8 were linear elastic during the operation of the dam. Therefore, the linear elastic model could be employed in numerical analysis, which required only 2 parameters, including Young's modulus (E'), Poisson's ratio (ν'). These parameters were taken from laboratory tests for the dam material and soil investigation report for the rock layers. The input parameters of the dam material and the rock layers were summarized in Table 3.

Table 3. Input parameters of dam material, soil and rock layers

Parameter	Symbol	Unit	Dam material	Rock layer 7	Rock layer 8
Unsaturated unit weight	γ_{unsat}	kN/m^3	25.9	25.3	25.5
Saturated unit weight	γ_{sat}	kN/m^3	25.9	25.3	25.5
Poisson's ratio	ν		0.21	0.37	0.33
Elastic modulus	E	kN/m^2	2.5x10^6	4x10^6	7x10^6

In order to validate the 3D numerical model, 4 storage levels were considered, including +294.50 m at the reservoir's dead storage level, +295.10 m at the 1st scanning campaign, +300.90 m at the 2nd scanning campaign, and +307.95 m at the 3rd scanning campaign. For simplicity, these storage levels were denoted as SL0, SL1, SL2, and SL3, respectively. The numerical phases were simulated as follows:

- Initial phase: the completed dam with dead water level (gravity loading analysis)
- Phase 1 (starting from intial phase): the completed dam with water level of +295.10 m (plastic analysis)
- Phase 2 (starting from intial phase): the completed dam with water level of +300.90 m (plastic analysis)
- Phase 3 (starting from intial phase): the completed dam with water level of +307.95 m (plastic analysis)

4 RESULTS AND DISCUSSION

The dam surface deformation along the stream direction was herein denoted as the horizontal deformation. Results calculated by numerical analysis was compared with those of measurement data at 3 typical cross-sections (TR1, TR2, and TR3). These cross-sections, shown in figure 7, were located mainly at the center of the dam where the maximum surface deformations took place. Figure 8 is the horizontal dam surface deformation at SL1 (+295.10 m). It can be seen that the dam exhibits significant deformations mostly at the center and the maximum deformation recorded is 3.7 cm. The deformation decreases from the center to the dam sides, which is attributed to the fixity at the boundaries of the dam. Since the scanning survey was performed at SL1, SL2, and SL3, the increase in the dam horizontal deformation was considered for comparison in two cases, i.e., SL2-SL1 and SL3-SL1. Figure 9 shows the deformation increment for SL2-SL1 case and SL3-SL1 case as calculated by numerical analysis and measured by the TLS at cross-section TR1, TR2, and TR3. In general, both the deformation increments by numerical analysis and the scanning survey show a cantilever shape with the maximum value at the top of the dam. At some points, the fluctuation of the scanned results can be observed due to the reflection of the pulsed laser close to the dam top. However, along the dam surface, the results by numerical analysis are very close to that of the scanning survey at all of the cross-sections. The maximum deformation increments are 1.0 cm and 1.7 cm corresponding to the SL2-SL1 and SL3-SL1 cases, respectively. The measurement data by total station was also added in figure 9 for comparison. The data are also in good agreement with the results by numerical analysis and the TLS. Therefore, the 3D numerical model of the dam is valid and can be employed to assess the stress state of the dam during operation. It should be emphasized that the calibration procedure will be more accurate if the number of scanning survey increases, e.g., with different storage water levels and different times.

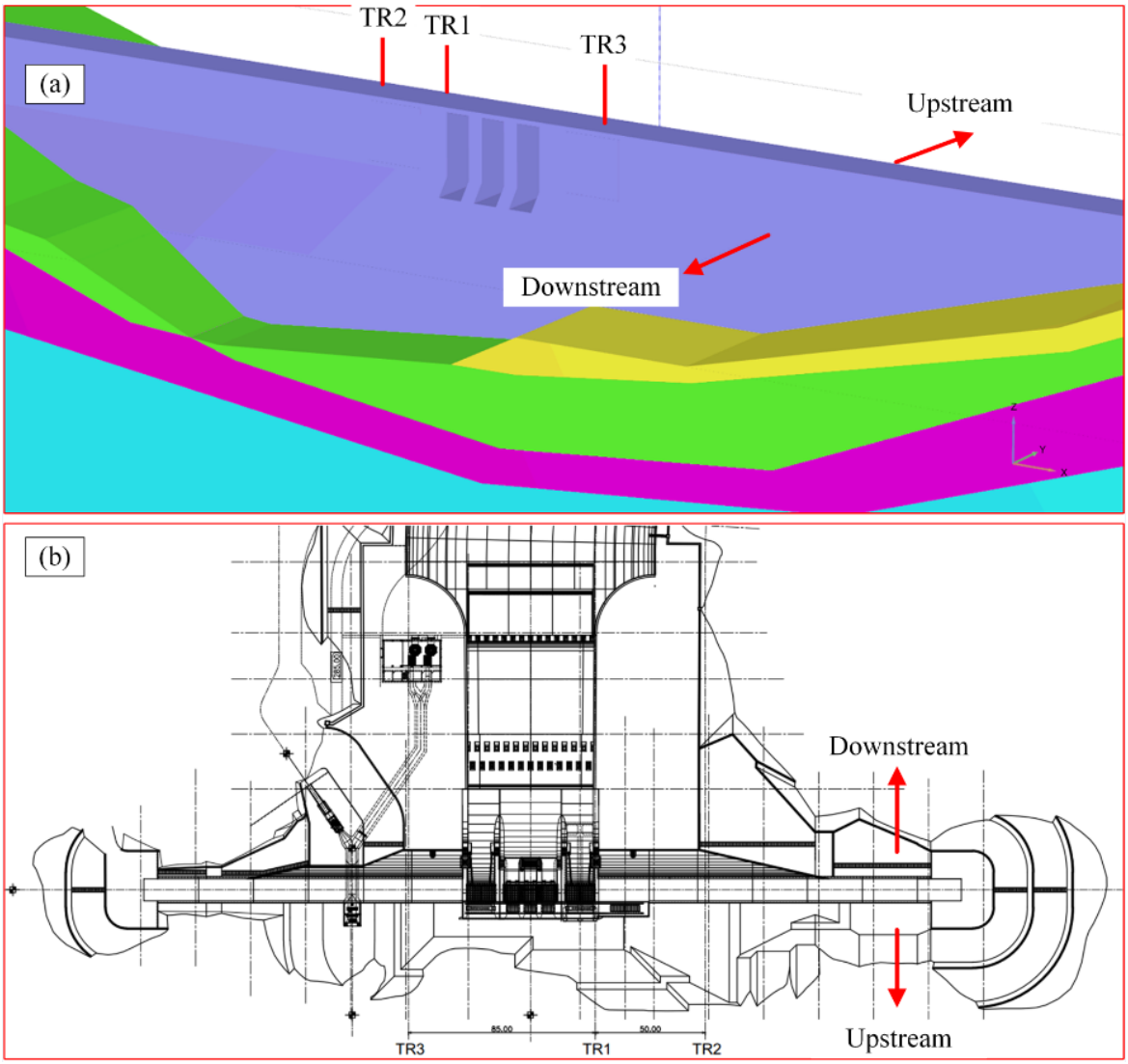

Figure 7. Locations of TR1, TR2, and TR3 cross sections at: (a) 3D model; (b) plan view

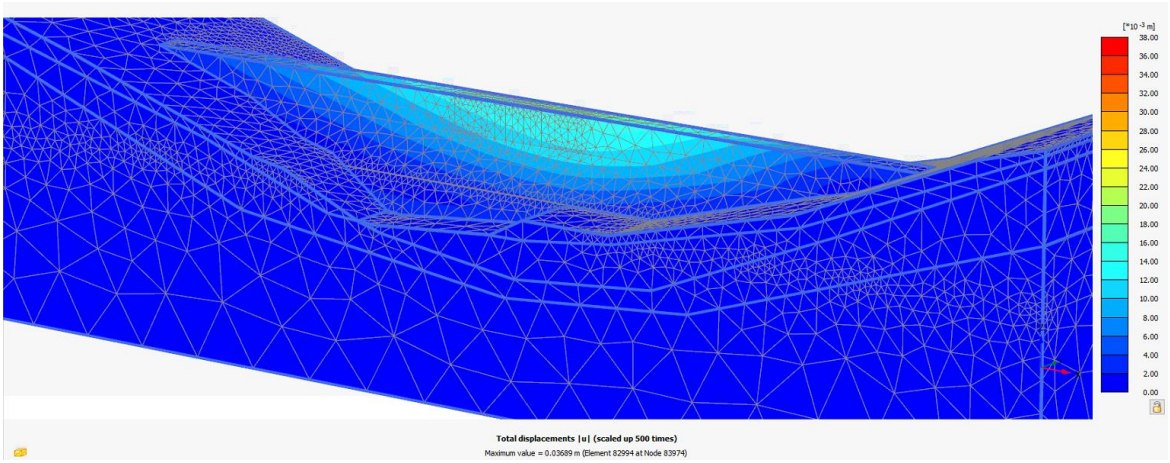

Figure 8. Dam surface deformation along the stream direction at SL1 (+295.10 m)

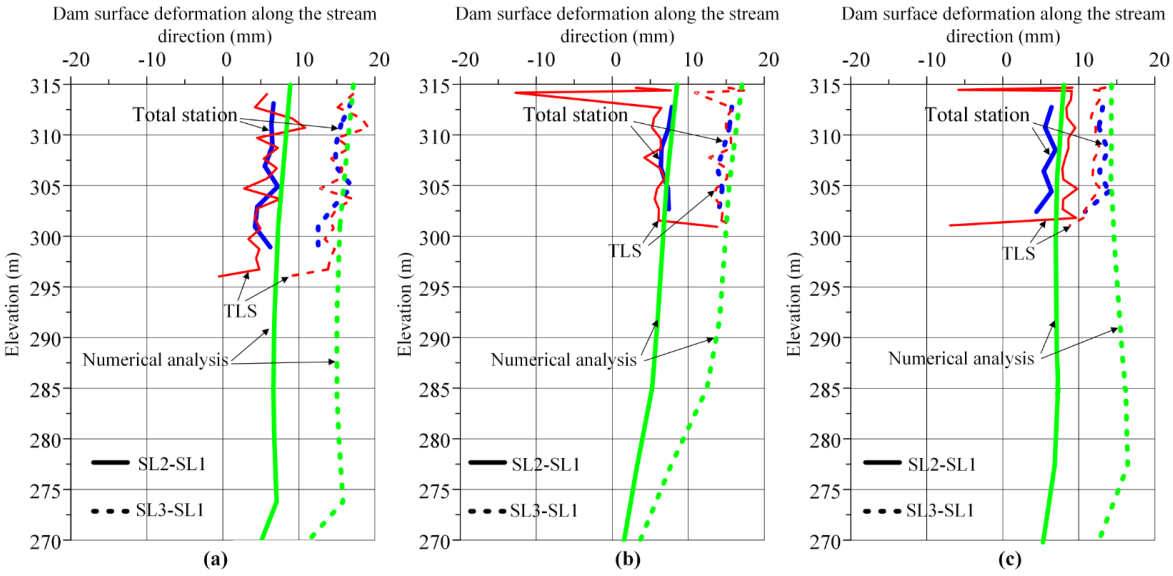

Figure 9. Comparison of dam surface deformation along the stream direction at (a) TR1; (b) TR2; (c) TR3

To investigate the stress state of the dam, numerical analysis was performed at various storage level, including the dead storage level (+294.50 m), normal storage level (+303.10 m), design flood level (+314.21 m), and check flood level (+314.25 m). Figure 10a is the vertical normal stress plot of the dam at the TR1 cross-section during the check flood level (+314.25 m), at which the compressive stress is negative, and the tensile one is positive. As shown in the figure, the vertical normal stress increases with depth along the dam and from the upstream to downstream side. The maximum and minimum vertical normal stresses within the dam body are 57.8 kN/m^2 and -436.1 kN/m^2, respectively. The horizontal normal stress plot along the stream direction at the TR1 cross-section during check flood level (+314.25 m) is shown in figure 10b. Within the dam body, the impact of the water pressure can be seen clearly at this plot, at which the maximum horizontal normal stress occurs at the downstream side (9.6 kN/m^2) and the minimum one takes place at the upstream side (-100.9 kN/m^2). The tensile horizontal normal stress distributes along the top upstream side of the dam. Also, along the dam foundation, the tensile horizontal normal stress concentrates at the upstream side. The distribution of stress state within the dam is compatible with the cantilever shape of the dam deformation. The relationship between the maximum and minimum vertical normal stresses and horizontal normal stresses along the stream diredction with storage water level is plotted in figure 11. In general, when the storage water level rises from +294.50 m to +314.25 m, the maximum (tensile) normal stresses reduces from +100 kN/m^2 to +10 kN/m^2 but the minimum (compressive) normal stresses decreases from -50 kN/m^2 to -450 kN/m^2. Since the dam material has maximum (tensile) and minimum (compressive) capacity of 710 kN/m^2 and -14400 kN/m^2, respectively, the dam can be evaluated as safe. Also, this relationship is helpful to roughly determine the normal stress generated in the dam corresponding to any storage water level during operation, at which one can judge the safety of the dam immediately.

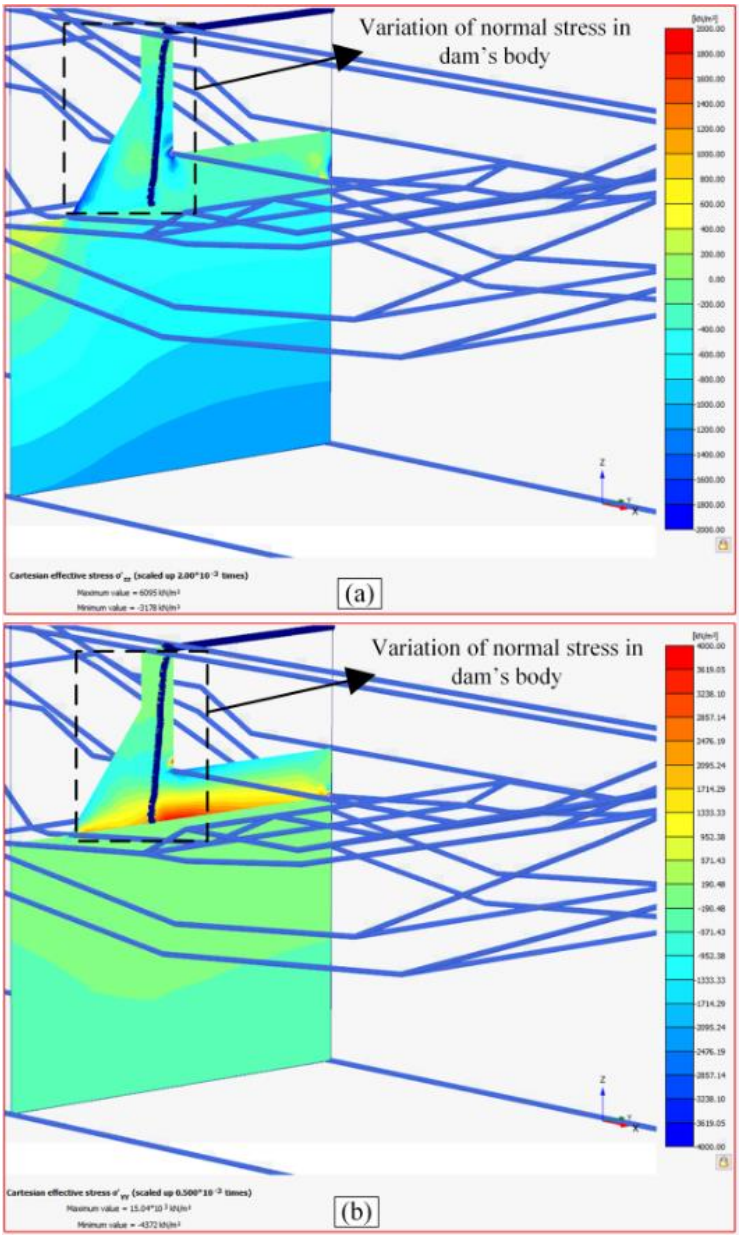

Figure 10. Normal stress plot at TR1 cross-section during check flood level (+314.25 m): (a) Vertical normal stress and (b) Horizontal normal stress along the stream direction

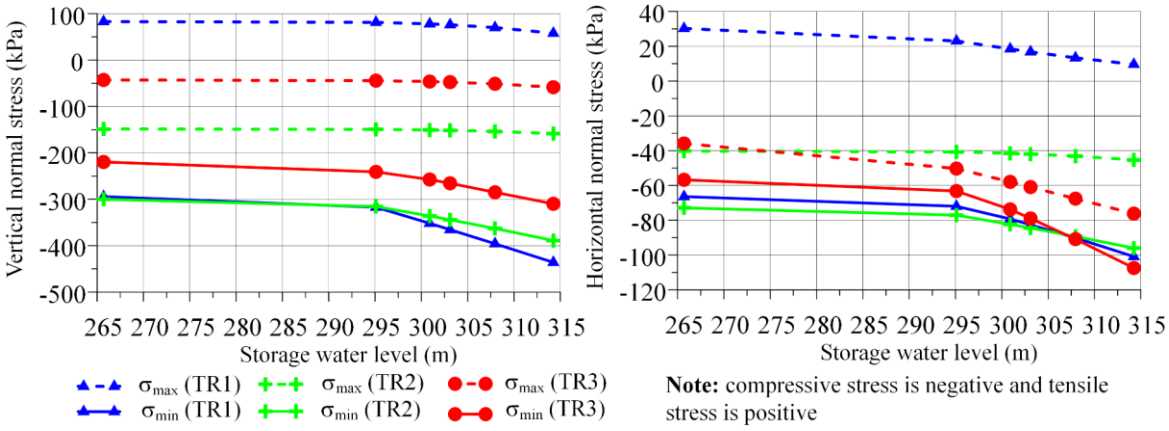

Figure 11. Relationship between maximum and minimum vertical normal stresses (a) and horizontal normal stresses along the stream diredction (b) with storage water level

Figure 12 shows a proposed flow chart to integrate results of the TLS and numerical analysis in assessing the safety of a dam in terms of normal stress during operation. It is suggested that a site investigation should be performed first, at which geometry of the studied dam, real topography, fluctuation of storage water level with time, and any obstacles are retrieved. Then, one can determine the layout of the scanning stations and schedule. Measurement data by other methods, such as total station, inclinometer, etc., are recommended to be employed to help calibrate results by TLS and 3D numerical analysis. The 3D numerical analysis should be calibrated continuously using the updated results of the TLS. Therefore, the stress state calculated by numerical analysis will be more accurate. The reason for that is the possible change in the properties of dam material and soil with time when the reservoir starts storing water.

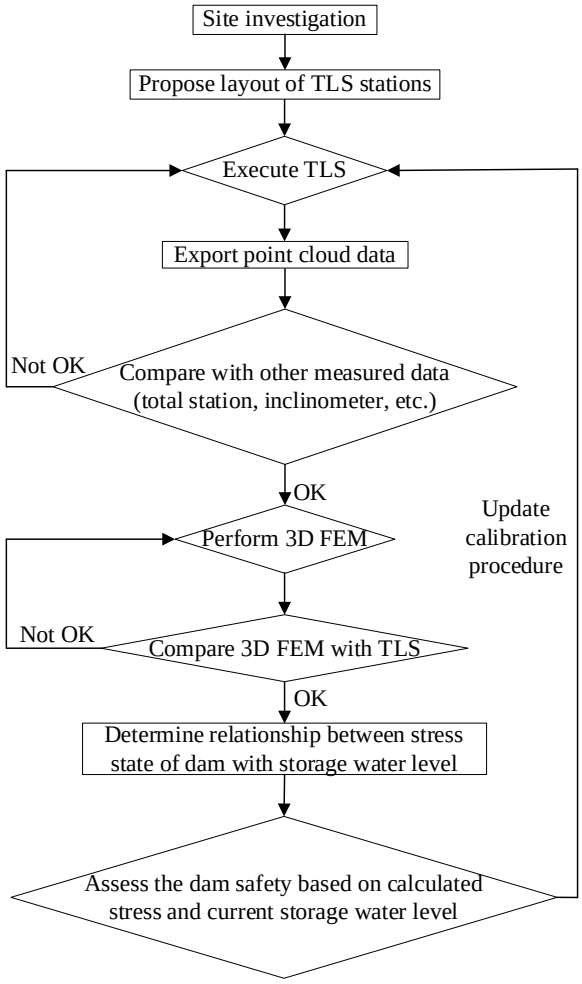

Figure 12. Flow chart of the integration between TLS and numerical analysis for dam safety assessment

5 CONCLUSIONS

On the basis of the above study, some conclusions can be drawn as follows:

i. TLS technique is suitable to be adopted for 3D scanning survey of dam in association with other measurement methods, such as total station, inclinometer, etc. This technique can generate point cloud data of a dam surface with maximum scanning rate of 120000 data points per second with overall standard deviation of 0.0008 m.
ii. The 3D finite element analysis can predict very accurately the dam's deformation. The difference between the calculated deformation and the measured one was only several millimeters. The relationship between the vertical normal stress and horizontal normal stress

along the stream direction of the dam with the storage water level can help to judge the safety of the dam immediately at any storage water level.

iii. A flow chart to integrate TLS data and 3D finite element analysis is proposed to assess the safety of other dams. In order to improve the accuracy of the prediction by this integration, it is suggested to employ measurement data by other methods, such as total station, inclinometer, etc. Also, the 3D numerical analysis should be calibrated continuously using the updated results of the TLS as the properties of the dam material and soil may change with time when the reservoir starts storing water.

ACKNOWLEDGMENTS

This research is funded by the Ministry of Agriculture and Rural Development (MARD) under the contract number 01/2023/HD-KHCN between Thuyloi University and the authors.

REFERENCES

Abellán, A., Vilaplana, J.M., Calvet, J., Garcíasellés, D., & Asensio, E., 2011. Rockfall monitoring by terrestrial laser scanning—Case study of the basaltic rock face at Castellfollit de la Roca (Catalonia, Spain). *Natural Hazards and Earth System Sciences*, 11(3), pp. 829–841. https://doi.org/10.5194/nhess-11-829-2011

Antova, G., 2015. Terrestrial laser scanning for dam deformation monitoring-case study. *Proceedings of FIG Working Week 2015*.

Aryan, A., Bosché, F., & Tang, T., 2021. Planning for terrestrial laser scanning in construction: A review. *Automation in Construction*, 125, 103551. https://doi.org/10.1016/j.autcon.2021.103551

Dai, B., Gu, C.S., Zhao, E.F., & Qin, X.N., 2018. Statistical model optimized random forest regression model for concrete dam deformation monitoring. *Structural Control and Health Monitoring*, 25(8), e2170. https://doi.org/10.1002/stc.2170

Ezzeldin, I., Naggar, H.E., & Newhook, J., 2024. Stresses induced in a buried corrugated metal arch culvert due to backfilling compaction efforts. *Tunnelling and Underground Space Technology*, 154, 106096. https://doi.org/10.1016/j.tust.2024.106096

Gu, H., Yang, M., Gu, C.S., & Huang, X.F., 2021, A factor mining model with optimized random forest for concrete dam deformation monitoring. *Water Science and Engineering*, 14(4), pp. 330–336. https://doi.org/10.1016/j.wse.2021.10.004

Gu, H., Yang, M., Gu, C.S., Cao, W.H., Huang, X.F., & Su, H.Z., 2020. An analytical approach of behavior change for concrete dam by panel data model. *Steel and Composite Structures*, 36(5), pp. 521–531. https://doi.org/10.12989/scs.2020.36.5.521

Gu, H., Yang, M., Gu, C.S., Fang, Z., Huang, & X.F., 2022. A comprehensive evaluation method for concrete dam health state combined with grayanalytic hierarchy-optimization theory. *Structural Health Monitoring*, 21(2), pp. 250–263. https://doi.org/10.1177/1475921721993388

He, J.P., Jiang, Z.X., Zhao, C., Peng, Z.Q., & Shi, Y.Q., 2018. CloudeVerhulst hybrid prediction model for dam deformation under uncertain conditions. *Water Science and Engineering*, 11(1), pp. 61–67. https://doi.org/10.1016/j.wse.2018.03.002

He, Q., Gu, C., Valente, S., Zhao, E., Liu, X., & Yuan, D., 2022. Multi-arch dam safety evaluation based on statistical analysis and numerical simulation. *Scientific Reports*, 12, 8913. https://doi.org/10.1038/s41598-022-13073-9

Hemeda, S., 2022. Geotechnical modelling and subsurface analysis of complex underground structures using PLAXIS 3D. *International Journal of Geo-Engineering*, 13 (9). https://doi.org/10.1186/s40703-022-00174-7

Hu, J., Wu, & S.H., 2019. Statistical modeling for deformation analysis of concrete arch dams with influential horizontal cracks. *Structural Health Monitoring*, 18(2), pp. 546–562. https://doi.org/10.1177/1475921718760309

Jiang, N., Li, H., Kou, Q., & Zhou, J., 2021. Quantitative monitoring method for analyzing the erosion of a landslide dam discharge channel using three-dimensional terrestrial laser scanning. *Geomatics, Natural Hazards and Risk*, 12(1), pp. 1905–1930. https://doi.org/10.1080/19475705.2021.1953157

Kaczmarek, H., Tyszkowski, S., Bartczak, A., Kramkowski, M., & Wasak, K., 2019. The role of freeze-thaw action in dam reservoir cliff degradation assessed by terrestrial laser scanning: A case study of Jeziorsko Reservoir (central Poland). *Science of the Total Environment*, 690, pp. 1140–1150. https://doi.org/10.1016/j.scitotenv.2019.07.032

Liu, H., & Kaynia, A.M., 2022. Monopile responses to monotonic and cyclic loading in undrained sand using 3D FE with SANISAND-MSu. *Water Science and Engineering*, 15(1), pp. 69–77. https://doi.org/10.1016/j.wse.2021.12.001

Ledesma, O., Sfriso, A., & Manzanal, D., 2022. Procedure for assessing the liquefaction vulnerability of tailings dams. *Computers and Geotechnics*, 144, 104632. https://doi.org/10.1016/j.compgeo.2022.104632

Maddah, A., Soroush, A., & Shafipour, R., 2021. A new concept for interpretation of building-excavation interaction in 3D conditions. *Tunnelling and Underground Space Technology*, 109, 103757. https://doi.org/10.1016/j.tust.2020.103757

Muralikrishnan, B., 2021. Performance evaluation of terrestrial laser scanners—a review. *Measurement Science and Technology*, 32(7). https://iopscience.iop.org/article/10.1088/1361-6501/abdae3

Oytun, M., & Atasoy, G., 2022. Effect of Terrestrial laser scanning (TLS) parameters on the accuracy of crack measurement in building materials. *Automation in Construction*, 144, 104590. https://doi.org/10.1016/j.autcon.2022.104590

Shen, N., Wang, B., Ma, H., Zhao, X., Zhou, Y., Zhang, Z., & Xu, J., 2023. A review of terrestrial laser scanning (TLS)-based technologies for deformation monitoring in engineering. *Measurement*, 223, 113684. https://doi.org/10.1016/j.measurement.2023.113684

Su, H.Z., Chen, Z.X., & Wen, Z.P., 2016. Performance improvement method of support vector machine-based model monitoring dam safety. *Structural Control and Health Monitoring*, 23(2), pp. 252–266. https://doi.org/10.1002/stc.1767

Su, H.Z., Li, X., Yang, B.B., & Wen, Z.P., 2018a. Wavelet support vector machine-based prediction model of dam deformation. *Mechanical Systems and Signal Processing*. 110, pp. 412–427. https://doi.org/10.1016/j.ymssp.2018.03.022

Su, H.Z., Ren, J., & Wen, Z.P., 2018b. An approach using Dempster–Shafer evidence theory to fuse multi-source observations for dam safety estimation. *Soft Computing*, 23, pp. 5633–5644. https://doi.org/10.1007/s00500-018-3220-z

TCVN 4253:2022. *Foundation of hydraulic projects - Requirements for design*.

Xu, H., Li, H., Yang, X., Qi, S., & Zhou, J., 2019. Integration of terrestrial laser scanning and nurbs modeling for the deformation monitoring of an earth-rock dam. *Sensors*, 19(1). https://doi.org/10.3390/s19010022

Xiao, P., Zhao, R., Li, D., Zeng, A., Qi, S., & Yang, X., 2022. As-built inventory and deformation analysis of a high rockfill dam under construction with terrestrial laser scanning. *Sensors*, 22 (2), pp. 521. https://doi.org/10.3390/s22020521

Yue, D., Wang, J., Zhou, J., Chen, X., & Ren, H., 2010. Monitoring slope deformation using a 3-D laser image scanning system: A case study. *Mining Science and Technology (China)*, 20(6), pp. 898–903. https://doi.org/10.1016/S1674-5264(09)60303-3

Zhan, M., Chen, B., & Wu, Z., 2023. Deformation warning index for reinforced concrete dam based on structural health monitoring data and numerical simulation. *Water Science and Engineering*, 16(4), pp. 408–418. https://doi.org/10.1016/j.wse.2023.09.002

Zhao, E.F., & Wu, C.Q., 2021. Risk probabilistic assessment of ultrahigh arch dams through regression panel modeling on deformation behavior. *Structural Control and Health Monitoring*, 28(5), e2716. https://doi.org/10.1002/stc.2716